HHS Public Access

Author manuscript

Angew Chem Int Ed Engl. Author manuscript; available in PMC 2018 September 18.

Published in final edited form as:

Angew Chem Int Ed Engl. 2017 September 18; 56(39): 11896–11900. doi:10.1002/anie.201703657.

Antimonene Quantum Dots: Synthesis and Application as Near-Infrared Photothermal Agents for Effective Cancer Therapy

Dr Wei Tao[+],
Center for Nanomedicine, Brigham and Women's Hospital, Harvard Medical School, Boston, MA 02115, United States

Xiaoyuan Ji[+],
Center for Nanomedicine, Brigham and Women's Hospital, Harvard Medical School, Boston, MA 02115, United States

Xiaoding Xu[+],
Center for Nanomedicine, Brigham and Women's Hospital, Harvard Medical School, Boston, MA 02115, United States

Dr. Mohammad Ariful Islam,
Center for Nanomedicine, Brigham and Women's Hospital, Harvard Medical School, Boston, MA 02115, United States

Zhongjun Li,
Shenzhen Engineering Laboratory of Phosphorene and Optoelectronics, SZU-NUS Collaborative Innovation Center for Op-toelectronic Science and Technology, and Key Laboratory of Optoelectronic Devices and Systems of Ministry of Education and Guangdong Province, Shenzhen University, Shenzhen 518060, China

Si Chen,
Shenzhen Engineering Laboratory of Phosphorene and Optoelectronics, SZU-NUS Collaborative Innovation Center for Op-toelectronic Science and Technology, and Key Laboratory of Optoelectronic Devices and Systems of Ministry of Education and Guangdong Province, Shenzhen University, Shenzhen 518060, China

Dr. Phei Er Saw,
Center for Nanomedicine, Brigham and Women's Hospital, Harvard Medical School, Boston, MA 02115, United States

Han Zhang,
Shenzhen Engineering Laboratory of Phosphorene and Optoelectronics, SZU-NUS Collaborative Innovation Center for Op-toelectronic Science and Technology, and Key Laboratory of Optoelectronic Devices and Systems of Ministry of Education and Guangdong Province, Shenzhen University, Shenzhen 518060, China

Zameer Bharwani,

Correspondence to: Han Zhang; Jinjun Shi; Omid C. Farokhzad.

[+]W. Tao, X. Ji, and X. Xu contributed equally to this work.

O.C.F. has financial interest in Selecta Biosciences, Tarveda Therapeutics, and Placon Therapeutics.

Center for Nanomedicine, Brigham and Women's Hospital, Harvard Medical School, Boston, MA 02115, United States

Zilei Guo,
Center for Nanomedicine, Brigham and Women's Hospital, Harvard Medical School, Boston, MA 02115, United States

Prof. Jinjun Shi*, and
Center for Nanomedicine, Brigham and Women's Hospital, Harvard Medical School, Boston, MA 02115, United States

Prof. Omid C. Farokhzad*
Center for Nanomedicine, Brigham and Women's Hospital, Harvard Medical School, Boston, MA 02115, United StatesKing Abdulaziz University, Jeddah 21589, Saudi Arabia

Abstract

Photothermal therapy (PTT) has shown significant potential for cancer therapy. However, developing nanomaterials (NMs)-based photothermal agents (PTAs) with satisfactory photothermal conversion efficacy (PTCE) and biocompatibility remains a key challenge. Herein, a new generation of PTAs based on two-dimensional (2D) antimonene quantum dots (AMQDs) was developed by a novel liquid exfoliation method. Surface modification of AMQDs with polyethylene glycol (PEG) significantly enhanced both biocompatibility and stability in physiological medium. The PEG-coated AMQDs showed a PTCE of 45.5%, which is higher than many other NMs-based PTAs such as graphene, Au, MoS_2, and black phosphorus (BP). The AMQDs-based PTAs also exhibited a unique feature of NIR-induced rapid degradability. Through both *in vitro* and *in vivo* studies, the PEG-coated AMQDs demonstrated notable NIR-induced tumor ablation ability. This work is expected to expand the utility of 2D antimonene (AM) to biomedical applications through the development of an entirely novel PTA platform.

TOC image

Antimonene quantum dots (AMQDs) were synthesized through a novel liquid exfoliation method. The PEG-coated AMQDs were demonstrated to have high photothermal conversion efficiency (45.5%), NIR-induced degradability, and biocompatibility, making them a new generation of ideal photothermal agents for effective cancer treatment. Our study opens up an exciting and novel research direction of AM for biomedical applications.

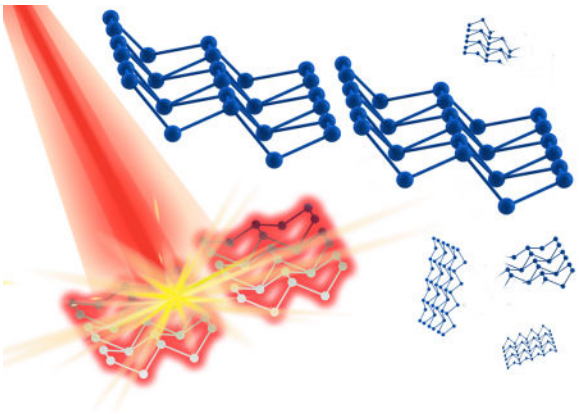

Keywords

two-dimensional; antimonene; quantum dots; photothermal agents; cancer therapy

Due to its minimal invasiveness and high selectivity, PTT has attracted considerable interest as a potent technique for cancer therapy.[1] However, synthesis of ideal PTAs has faced considerable challenges. One limitation is that few PTAs possess the requisite absorption spectra for NIR photothermal transduction.[2] The emerging 2D NMs with exciting physical and chemical properties can offer new solutions to this absorption constraint.[3] Examples include graphene derivatives (*e.g.*, graphene oxide, reduced graphene oxide)[4] and TMDs (*e.g.*, MoS_2, WS_2).[5] However, concerns about these materials' safety and biocompatibility persist. Similar problems exist for other inorganic PTAs such as noble-metal NMs (*e.g.*, Au and Ag),[6] carbon nanotubes,[7] and Cu-based materials.[8] While organic PTAs were intended to reduce concerns relevant to inorganic PTAs, most of them are still subject to various limitations including complicated fabrication, indistinct degradation, and potential biosafety concerns.[9] Therefore, the development of novel NMs-based PTAs is of vital significance and clinical value.

AM is a recently described 2D layered material[10] that can be simply exfoliated from bulk antimony (Sb) and has recently received increasing interest due to its superior physicochemical properties compared with typical 2D NMs (*e.g.*, graphene, MoS_2, WS_2, and BP).[11] Because of its similarity to these 2D NMs, AM possesses great potential for development as a PTA. Notably, antimonial drugs have also been used in medicine for several centuries.[12] Hence, we expected that AM may have excellent photothermal effects similar to those of emerging 2D NMs, while potentially holding more promise for clinical translation. However, the application of AM in biomedicine remains unexplored, let alone reports on using 2D AM-based materials as PTAs.

Herein, novel 2D AMQDs were synthesized and their potential as PTAs was explored. We developed a simple liquid exfoliation strategy for the synthesis of highly dispersed ultrasmall AMQDs (Figure 1a, b), which involves ultrasound probe sonication together with ice-bath sonication in ethanol. Compared to traditional liquid exfoliation with single-probe sonication, our 2-step combined sonication strategy produces ultrasmall uniform particles

with little batch-to-batch variability. Due to the electron screening effect, bare AMQDs aggregate and precipitate in the presence of salts. To enhance the stability and dispersity of AMQDs in physiological medium, 1,2-Distearoyl-sn-glycero-3-phosphoethanolamine-N-[methoxy(poly ethylene glycol)] (DSPE-PEG) was utilized to coat their surface via both van der Waals forces and hydrophobic interactions. As presented in Figure S1, PEG-coated AMQDs showed negligible agglomeration after 48 h of incubation and remarkably better stability in phosphate-buffered saline (PBS) and cell culture medium compared to bare AMQDs.

Next, AMQDs and PEG-coated AMQDs were characterized by several methods. As shown in the transmission electron microscopy (TEM) and atomic force microscopy (AFM) images below, the average size of AMQDs was ~2.8 nm, and the average thickness was ~1.6 nm (Figure S2). The chemical compositions of AMQDs were confirmed by X-ray photoelectron spectroscopy (XPS). As shown in Figure S3 and S4, there were O and Sb elements in the XPS survey spectrum of AMQDs. For PEG-coated AMQDs, the average size was ~3.9 nm and the average thickness was ~2.6 nm (Figure 1c–f). This slight increase in the size and thickness resulted from the PEG coating.[5b, 13] Fourier transform infrared spectrum (FT-IR) was also applied to identify the chemical compositions of AMQDs pre- and post-PEG coating. In the FTIR spectrum (Figure 1g), the absorption bands at ~2900 cm^{-1} were attributable to the CH vibration and those at ~1650–1660 cm^{-1} were attributable to C=O stretching vibrations in the DSPE-PEG segment. These bands indicate the successful PEG coating of AMQDs. The crystal structure of AMQDs and PEG-coated AMQDs was further confirmed by Raman spectra and X-ray diffractometry (XRD). The Raman spectra of exfoliated AMQDs (Figure 1h) showed peaks similar to bulk Sb (~108 and 147 cm^{-1}), which was similar to previous report.[10b] A slight shift was found after PEG coating, which could be the result of a slight increase in thickness after the addition of the PEG coating.[13b, 14] The amount of DSPE-PEG that was coated on the AMQDs' surface was ~51.5% (w/w%) of the AMQDs. As shown in XRD spectra (Figure 1i), the AMQDs pre- and post-PEG coating could be indexed as hexagonal antimonene consistent with JCPDS No. 35-0732.

To explore the potential of AMQDs-based NMs as PTAs, three vital factors (*i.e.*, PTCE, degradability, and biocompatibility) were checked. First, PTT employs PTAs to absorb light and convert it into heat for tumor ablation, making strong absorption in the NIR region of PTAs crucial. Encouragingly, both AMQDs and PEG-coated AMQDs exhibited broad and strong absorption, ranging from ultraviolet (UV) to NIR wavelengths (Figure S5, 6). This also confirmed that the surface PEG coating did not affect NIR absorbance. Subsequently, PTCE was evaluated by exposing aqueous solutions of PEG-coated AMQDs with different concentrations to an 808 nm NIR laser. The photothermal heating curves (Figure 2a, S7–8) showed a strong concentration-dependent photothermal effect for PEG-coated AMQDs, with the highest temperature increment (ΔT) up to 50 °C at a concentration of 200 μg/mL. In contrast, insignificant heating (a temperature rise of only ~4 °C) was observed for water. Furthermore, the PTCE (η) of PEG-coated AMQDs was calculated according to previous methods[15] as follows:

$$\eta = \frac{hA\Delta T_{max} - Q_s}{I\left(1 - 10^{-A_{808}}\right)} \quad (1)$$

where h is the coefficient of heat transfer, A is the container surface area, ΔT_{max} is the maximum temperature change of the PEG-coated AMQDs solution, I is the power density of the NIR laser, A_{808} is the absorbance of the solution of PEG-coated AMQDs at 808 nm, and Q_s is the heat associated with the light absorbance of the water. According to Equation 1, the η value of PEG-coated AMQDs was determined to be 45.5%, which is higher than majority of NMs-based PTAs such as Au nanoshells (13%), Au nanorods (21%), Graphene Oxide (25%), $Cu_{2-x}Se$ nanoparticles (22%), MoS_2-PEG nanoflakes (27.6%), BPQDs (28.4%), Sb nanorod bundles (41%), Bi_2S_3 nanorods (28.1%), or Bi_2Se_3 nano-spherical sponges (31.1%) (Table S1).[13b, 16] The high η value of PEG-coated AMQDs makes them quite promising as PTAs.

It has also been considered that NIR-induced degradation of photothermal nanomaterials (*e.g.*, BP) could highlight their application in biological areas since they could be degraded after therapeutic effects are achieved.[17] We utilized previously reported methods[17–18] to assess the NIR-induced degradability of AMQD-based PTAs in water. Dispersions of AMQDs and PEG-coated AMQDs were exposed to an 808 nm NIR laser for 5 min, followed by natural cooling to room temperature. This cycle was repeated 3–4 times. As shown in Figure S9a and S9d, the dark colors of both AMQDs and PEG-coated AMQDs faded until becoming nearly transparent during the irradiation cycles, suggesting that the 2D nanomaterials might have been substantially degraded by the laser. This could also be confirmed by the UV-Vis-NIR absorbance spectra (Figure S9b–f). Moreover, the NIR-induced degradation of AMQD-based PTAs appears significantly superior to that of BP, since the latter takes more than 2 weeks to be degraded,[17] and AMQD-based PTAs took only minutes in our study. Notably, the NIR-induced degradation was strongly dependent on water, since such degradability was not observed in ethanol (Figure S10–11).

Biocompatibility is also requisite for PTAs used in biomedicine. Therefore, the cytotoxicity of the PEG-coated AMQDs was evaluated in a panel of normal and cancer cells *in vitro*. As Figure 3a shows, no obvious cytotoxicity could be observed, indicating their potential biocompatibility. We next investigated the NIR-mediated *in vitro* cytotoxicity of AMQDs in MCF-7 and HeLa cells (Figure 3b and S12). Cells were exposed to AMQDs for 4 hrs, allowing for uptake, and then irradiated with an 808 nm laser for 5 min. Cellular viability significantly decreased as the concentration of PEG-coated AMQDs increased in both cell lines, with <10% of cells viable at 200 μg/mL. We also directly demonstrated the superior therapeutic effect through a live/dead cell co-staining study. As expected, only the cells exposed to laser irradiation (within the black shadow; Fig 3c) were killed, and a clear demarcation line between live cells (green) and dead cells (red) was observed in both cell lines (Figure 3d–f and S13). In marked contrast, there was negligible death among cells treated with only NIR or only PEG-coated AMQDs (Figure S14–15). These findings further confirm the good biocompatibility of PEG-coated AMQDs and indicate that combining PEG-coated AMQDs with NIR irradiation can effectively kill cancer cells by PTT.

Finally, *in vivo* therapeutic studies and biocompatibility evaluations were carried out. MCF-7 subcutaneous xenograft nude mice were treated with saline (G1), NIR irradiation (G2), PEG-coated AMQDs (G3), or PEG-coated AMQDs with subsequent NIR irradiation (G4) after intratumor (i.t.) injection. G2 and G4 were treated with an 808 nm laser at 1 W cm^{-2} for 10 min at tumor sites. ΔT was monitored during irradiation using an IR thermal camera (Figure 4a–b). After 10 min irradiation, ΔT of G2 was only ~5 °C, while that of G4 was >30 °C, achieving significant temperature rises throughout the irradiation period. The tumors in G1–G3 grew quickly, suggesting that "only NIR" or "only PEG-coated AMQDs" had no more effect on inhibiting tumor growth than the control group (G1). In contrast, tumors in G4 were ablated after PTT with negligible growth or no regrowth (Table S2 and Figure 4c). All mice were euthanized and representative tumors were collected (Figure 4d). Meanwhile, our preliminary studies found that different treatments with PEG-coated AMQDs had no influence on body weight changes or caused tissue damage (Figure S16–17). To further show the potential of the PEG-coated AMQDs for cancer PTT, we also tested their *in vivo* performance after intravenous (i.v.) injection. The PEG-coated AMQDs showed a relatively long blood circulation (Figure S18a) and high accumulation at the tumor sites (Figure S18b–c), which is similar as other reported QDs of similar size.[19] The strong PTT efficacy was also confirmed by the complete ablation of tumors after i.v. injection (Figure S18d–e). In addition, all the parameters in the serum biochemistry and complete blood panel tests were within normal ranges after i.v. injection of PEG-coated AMQDs during the monitoring period (Figure S19). These data together suggest the excellent PTT efficacy and biocompatability of our PEG-coated AMQDs *in vivo*.

In summary, we successfully developed novel AMQDs-based PTAs by a controllable liquid exfoliation method. The prepared PEG-coated AMQDs exhibited excellent stability in physiological environments, superior NIR photothermal performance with a PTCE of 45.5%, and no obvious toxicity in a panel of cells at the tested concentrations. The differently structured 2D AMQDs not only achieved significant PTCE similar to previously reported semimetal Sb nanorod bundles (200-300 nm long and 50–80 nm thick)[16c], but also demonstrated rapid NIR-induced degradability, which could further highlight their biomedical applications[17]. In addition, the PEG-coated AMQDs also showed excellent NIR light-induced tumor ablation and biocompatibility *in vivo*. It is worth mentioning that As, Bi, and Sb all belong to the VA group of elements with layer-by-layer structure,[20] and thus analogous methods may also be utilized to generate 2D layered elemental materials (*e.g.*, arsenene and bismuthene) with ultrasmall size in suitable exfoliation solutions. We expect this study to open up an exciting research direction for 2D AM and its combination with other nano-platforms in biomedical applications.

Supplementary Material

Refer to Web version on PubMed Central for supplementary material.

Acknowledgments

This work was supported by NIH grants HL127464 (O.C.F.), CA200900 (J.S.) and R00CA160350 (J.S.); the David H. Koch-Prostate Cancer Foundation (PCF) Program in Cancer Nanotherapeutics (O.C.F.); the National Research Foundation of Korea grant K1A1A2048701 (O.C.F.); NSFC grants 61435010 and 61575089 (H.Z.); NSF of

Grangdong Province grant 2016A030310023 (W.T.); STIC of Shenzhen grants KQTD2015032416270385 and JCYJ20150625103619275 (H.Z. and W.T.).

References

1. a) Shi J, Kantoff PW, Wooster R, Farokhzad OC. Nat Rev Cancer. 2017; 17:20–37. [PubMed: 27834398] b) Kievit FM, Zhang M. Acc Chem Res. 2011; 44:853–862. [PubMed: 21528865] c) Miao W, Kim H, Gujrati V, Kim JY, Jon H, Lee Y, Choi M, Kim J, Lee S, Lee DY, Kang S, Jon S. Theranostics. 2016; 6:2367–2379. [PubMed: 27877241] d) Song J, Wang F, Yang X, Ning B, Harp MG, Culp SH, Hu S, Huang P, Nie L, Chen J, Chen X. J Am Chem Soc. 2016; 138:7005–7015. [PubMed: 27193381] e) Huang P, Lin J, Li W, Rong P, Wang Z, Wang S, Wang X, Sun X, Aronova M, Niu G, Leapman RD, Nie Z, Chen X. Angew Chem Int Ed Engl. 2013; 52:13958–13964. [PubMed: 24318645] f) Chen H, Zhang W, Zhu G, Xie J, Chen X. Nat Rev Mater. 2017; 2:17024.
2. Xuan J, Wang Z, Chen Y, Liang D, Cheng L, Yang X, Liu Z, Ma R, Sasaki T, Geng F. Angew Chem Int Ed Engl. 2016; 128:14789–14794.
3. Chen Y, Wang LZ, Shi JL. Nano Today. 2016; 11:292–308.
4. a) Yang K, Feng L, Shi X, Liu Z. Chem Soc Rev. 2013; 42:530–547. [PubMed: 23059655] b) Jiang T, Sun W, Zhu Q, Burns NA, Khan SA, Mo R, Gu Z. Adv Mater. 2015; 27:1021–1028. [PubMed: 25504623]
5. a) Cheng L, Yuan C, Shen S, Yi X, Gong H, Yang K, Liu Z. ACS Nano. 2015; 9:11090–11101. [PubMed: 26445029] b) Liu T, Wang C, Gu X, Gong H, Cheng L, Shi X, Feng L, Sun B, Liu Z. Adv Mater. 2014; 26:3433–3440. [PubMed: 24677423]
6. Jain PK, Huang X, El-Sayed IH, El-Sayed MA. Acc Chem Res. 2008; 41:1578–1586. [PubMed: 18447366]
7. Wang X, Wang C, Cheng L, Lee ST, Liu Z. J Am Chem Soc. 2012; 134:7414–7422. [PubMed: 22486413]
8. Tian Q, Tang M, Sun Y, Zou R, Chen Z, Zhu M, Yang S, Wang J, Wang J, Hu J. Adv Mater. 2011; 23:3542–3547. [PubMed: 21735487]
9. Zou Q, Abbas M, Zhao L, Li S, Shen G, Yan X. J Am Chem Soc. 2017; 139:1921–1927. [PubMed: 28103663]
10. a) Gibaja C, Rodriguez-San-Miguel D, Ares P, Gomez-Herrero J, Varela M, Gillen R, Maultzsch J, Hauke F, Hirsch A, Abellan G, Zamora F. Angew Chem Int Ed Engl. 2016; 55:14345–14349. [PubMed: 27529687] b) Pizzi G, Gibertini M, Dib E, Marzari N, Iannaccone G, Fiori G. Nat Commun. 2016; 7:12585. [PubMed: 27557562]
11. a) Ares P, Aguilar-Galindo F, Rodríguez-San-Miguel D, Aldave DA, Díaz-Tendero S, Alcamí M, Martín F, Gómez-Herrero J, Zamora F. Adv Mater. 2016; 28:6332–6336. [PubMed: 27272099] b) Ji J, Song X, Liu J, Yan Z, Huo C, Zhang S, Su M, Liao L, Wang W, Ni Z. Nat Commun. 2016; 7:13352. [PubMed: 27845327]
12. Frezard F, Demicheli C, Ribeiro RR. Molecules. 2009; 14:2317–2336. [PubMed: 19633606]
13. a) Cheng L, Liu J, Gu X, Gong H, Shi X, Liu T, Wang C, Wang X, Liu G, Xing H, Bu W, Sun B, Liu Z. Adv Mater. 2014; 26:1886–1893. [PubMed: 24375758] b) Sun Z, Xie H, Tang S, Yu XF, Guo Z, Shao J, Zhang H, Huang H, Wang H, Chu PK. Angew Chem Int Ed Engl. 2015; 3:11526–11530.
14. Tao W, Zhu X, Yu X, Zeng X, Xiao Q, Zhang X, Ji X, Wang X, Shi J, Zhang H, Mei L. Adv Mater. 2017; 29:1603276.
15. Roper DK, Ahn W, Hoepfner M. J Phys Chem C. 2007; 111:3636–3641.
16. a) Hessel CM, Pattani VP, Rasch M, Panthani MG, Koo B, Tunnell JW, Korgel BA. Nano Lett. 2011; 11:2560–2566. [PubMed: 21553924] b) Wang B, Wang JH, Liu Q, Huang H, Chen M, Li K, Li C, Yu XF, Chu PK. Biomaterials. 2014; 35:1954–1966. [PubMed: 24331707] c) Li W, Rong P, Yang K, Huang P, Sun K, Chen X. Biomaterials. 2015; 45:18–26. [PubMed: 25662491]
17. Wang H, Yang X, Shao W, Chen S, Xie J, Zhang X, Wang J, Xie Y. J Am Chem Soc. 2015; 137:11376–11382. [PubMed: 26284535]
18. Shao J, Xie H, Huang H, Li Z, Sun Z, Xu Y, Xiao Q, Yu XF, Zhao Y, Zhang H, Wang H, Chu PK. Nat Commun. 2016; 7:12967. [PubMed: 27686999]

19. Nurunnabi M, Khatun Z, Huh KM, Park SY, Lee DY, Cho KJ, Lee YK. ACS Nano. 2013; 7:6858–6867. [PubMed: 23829293]

20. a) Pumera M, Sofer Z. Adv Mater. 2017; 29:1605299.b) Zhang S, Yan Z, Li Y, Chen Z, Zeng H. Angew Chem Int Ed Engl. 2015; 54:3112–3115. [PubMed: 25564773]

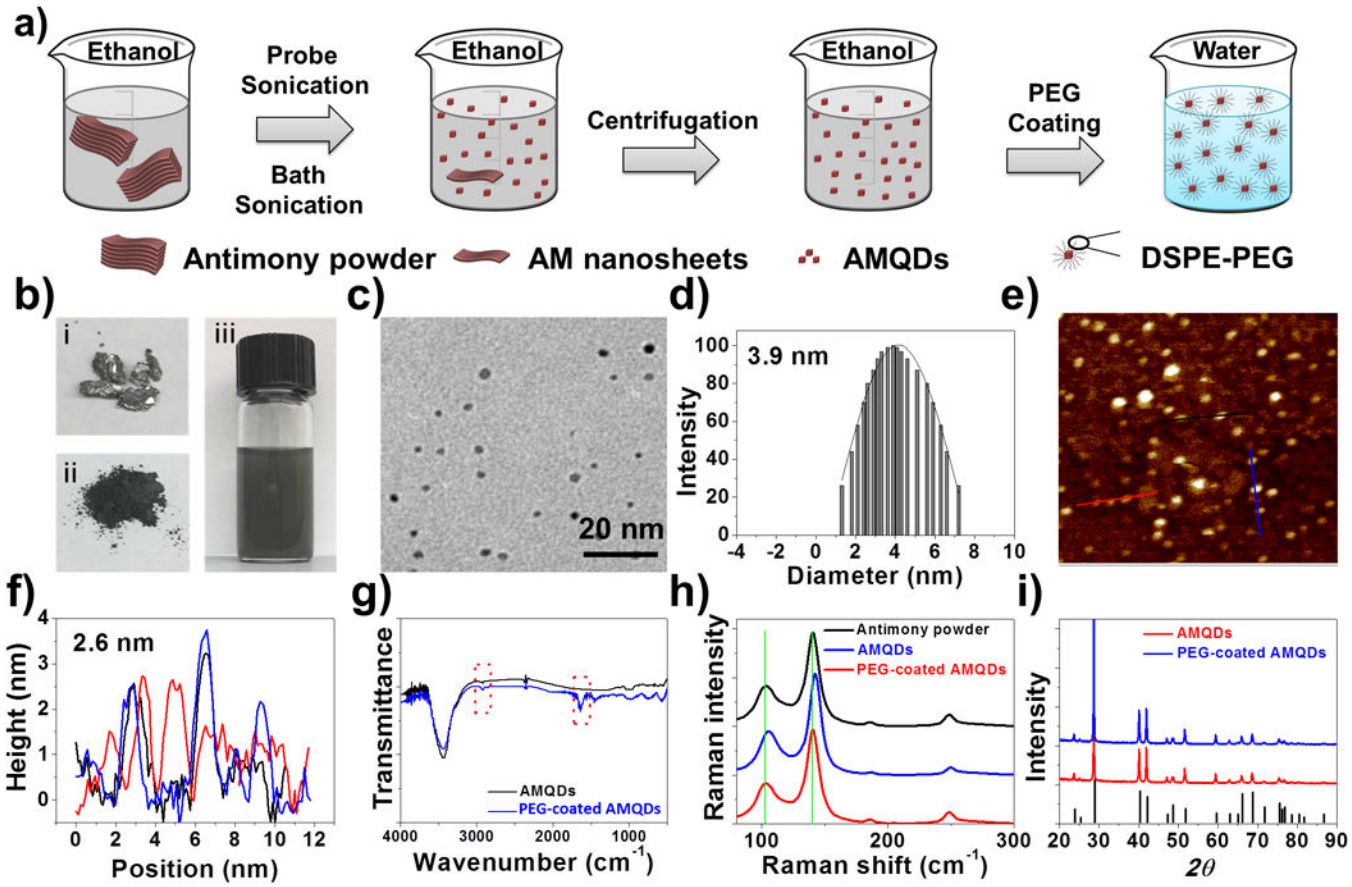

Figure 1.

a) Fabrication of PEG-coated AMQDs. b) photos of bulk antimony, antimony powder, and AMQDs solution during the preparation process, c) TEM image, d) diameter distribution, e) AFM image, and f) thickness of the PEG-coated AMQDs, g) FTIR spectrum, h) Raman spectrum, and i) XRD spectrum of AMQDs and PEG-coated AMQDs.

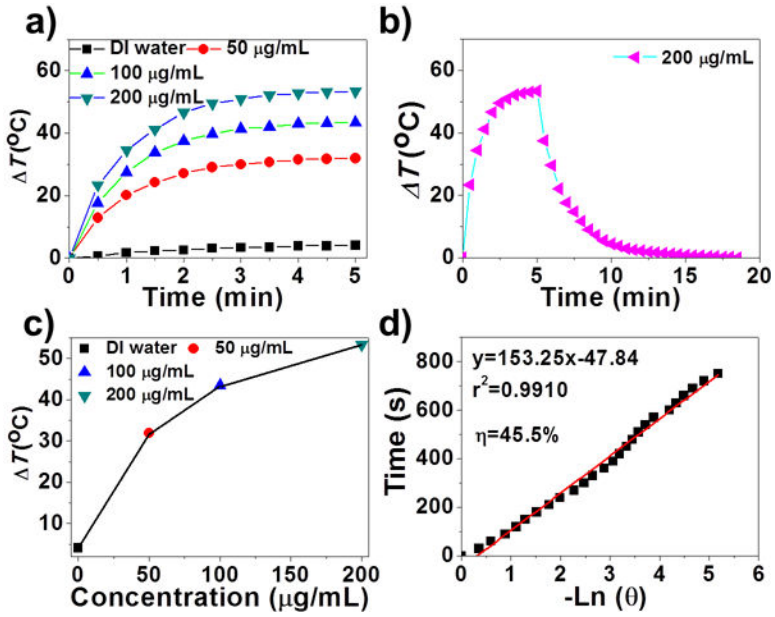

Figure 2.

a) Time-dependent temperature change during irradiation (808 nm, 2 W cm^{-2}). b) The photothermal heating curve of the PEG-coated AMQDs under irradiation and the cooling curve after turning off the laser. c) The temperature change (ΔT) for 5 min irradiation with different concentrations of PEG-coated AMQDs. d) Linear relationship between -ln θ and time obtained from the cooling time of (c).

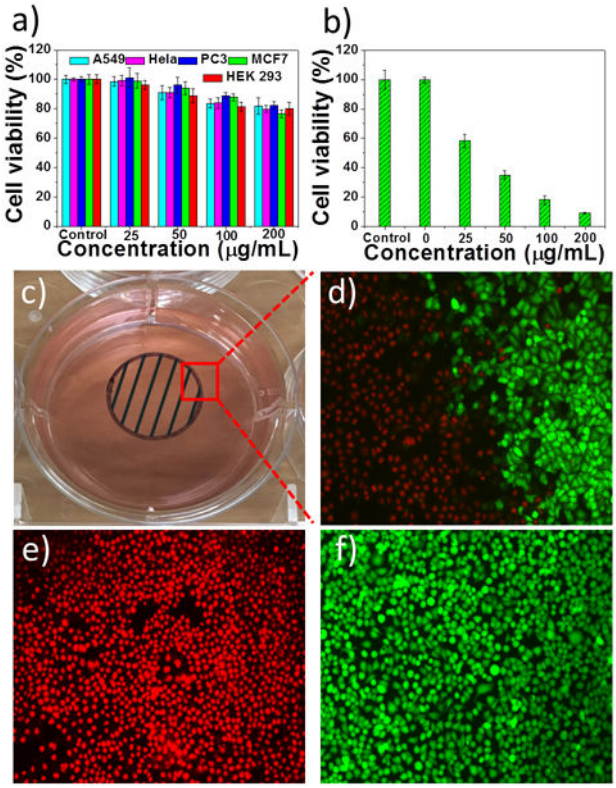

Figure 3.

a) Cell viability after incubation with only PEG-coated AMQDs. b) Cell viability of MCF-7 cells treated with PEG-coated AMQDs with NIR (808 nm, 1 W cm^{-2}) for 5 min. c) A photo of the cell culture dish after incubation with PEG-coated AMQDs. The black circle with shadow shows the laser spot. d-f) Confocal images of calcein AM (green, live cells) and PI (red, dead cells) co-stained MCF-7 cells after exposed to NIR irradiation (808 nm, 1 W cm^{-2}). The amplification of confocal images is 100×.

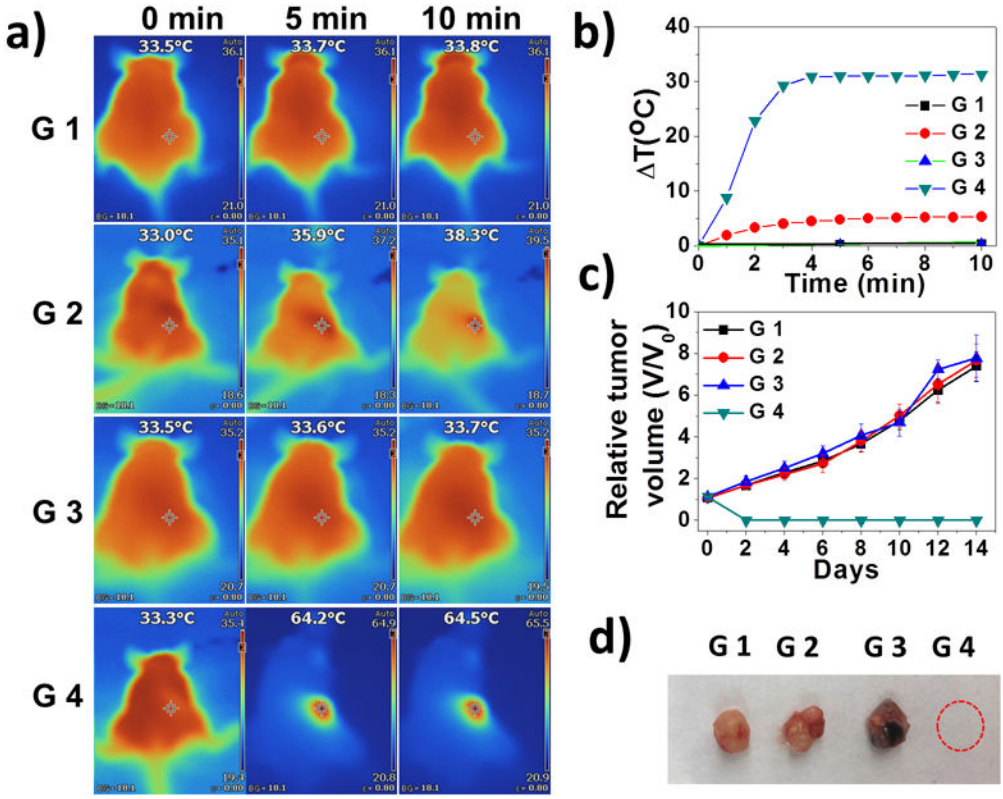

Figure 4.

a) IR images of MCF-7 tumor-bearing mice (G1: Saline; G2: only NIR; G3: only PEG-coated AMQDs; G4: PEG-coated AMQDs + NIR; 808 nm, 1 W cm^{-2}). b) Temperature changes at tumor sites. c) Relative tumor volumes after various treatments. d) Representative images of harvested tumors from each group at day 14.